Architecture and Conformation of Uncharged and Charged Hyperbranched Polymers: Computer Simulation and Mean-Field Theory

T. Mulder,* A. V. Lyulin, Paul van der Schoot, and M. A. J. Michels

Group Polymer Physics, Eindhoven Polymer Laboratories and Dutch Polymer Institute, Technische Universiteit Eindhoven, P.O. Box 513, 5600 MB Eindhoven, The Netherlands

Received February 26, 2004; Revised Manuscript Received November 18, 2004

ABSTRACT: The conformational behavior of both uncharged and charged hyperbranched polymers (HBPs) in dilute solutions has been studied using Brownian dynamics simulations. A distinction has been made between two types of architectures: type 1, which is characterized by its degree of polymerization (N) and its number of generations (g_{max}), and type 2, which is characterized by its degree of polymerization (N) and its degree of branching (DB). The radius of gyration (R_g) of both uncharged and charged type 1 HBPs is strongly influenced by variation of g. For uncharged type 2 HBPs R_g is relatively insensitive to variation of DB, whereas for charged type 2 HBPs R_g is a decreasing function of DB. The values of the radii of gyration as determined in the simulations are well reproduced in mean-field calculations. Scaling of R_g with the Wiener index and N has been investigated and compared to data from literature. The radial mass distribution of a charged type 1 HBP exhibits an ordering of the monomers that is highly dependent on g; the radial mass distribution of a charged type 2 HBPs shows an ordering that is only weakly dependent on DB. These orderings manifest themselves via oscillations of the static structure factor.

1. Introduction

In recent years a lot of research has been done on dendrimers. Dendrimers are perfect monodisperse macromolecules with a regularly and highly branched three-dimensional structure. According to a pioneering analytical theory of De Gennes and Hervet[1] for a dendrimer in a good solvent, the monomer density increases monotonically from the core to the periphery. On the contrary, Boris and Rubinstein[2] found, using a self-consistent mean-field model, that the density decreases monotonically from the center. Their results have been confirmed by various simulational studies.[3−6] Evers et al.[3] refined the model of Boris and Rubinstein by replacing their two-body interactions by multibody interactions and by accounting for deviations from Gaussian statistics at high chain stretching. While in a good solvent the internal configuration is quite open, in a poor solvent a dendrimer adopts a globular configuration with all monomers packed close together.[4] This solvent quality dependence of its configuration makes dendrimers ideal for guest−host chemistry.[7,8] Furthermore, dendrimers possess a very high end group functionality, which would make them adequate for catalysis or surface-activity purposes if the end groups would be located at the dendrimer's surface. The small-angle neutron scattering study of Rosenfeldt et al.[9] and the Brownian dynamics simulation of Lyulin et al.[10] demonstrated penetration of the higher generation monomers into the central region for neutral dendrimers. Monte Carlo simulations of Welch and Muthukumar[8,11] revealed the possibility of tuning the intramolecular density profile for polyelectrolytic dendrimers by changing the pH of the solvent. The significant influence of terminal charges on the radial density profile of dendrimers was also found by Evers et al.,[3] who performed Brownian dynamics simulations and mean-field calculations. The density profile exhibited maxima and minima that were induced by Coulomb interactions between charged end groups. The end groups were shown to be at the periphery.

Dendrimers can be synthesized either in a convergent or in a divergent method.[7] In the divergent method the synthesis is started with a multifunctional core molecule and elaborated to the periphery. Convergent methods start at the periphery and end at the core. Both methods consist primarily of a repetition of the following steps: attaching one generation to the other, purifying, and then changing functional groups for the next stage of the reaction. Replacing the many-steps synthesis procedure with a one-step polycondensation reaction, which is economically far more attractive, leads to a loss of control over molecular mass and size. The final product changes from dendrimers to hyperbranched polymers (HBPs). HBPs are characterized by nonideally, irregularly branching arrays, in which not every repeat unit contains a branching juncture, resulting in polydisperse sizes, shapes, masses, and topologies.

The simplicity of the polycondensation reaction in which HBPs are produced as compared to the many-steps procedure that is required to create dendrimers led to the question of whether HBPs practically show the same behavior as their dendrimer counterparts. A crucial point in investigations to answer this question is the way HBPs are characterized. Two useful topological parameters that are determinant for various quantities are the degree of branching (DB) and the Wiener index (W). DB is defined by Widmann et al.[12] as

$$DB = \frac{2D}{2D + L} \tag{1}$$

where D is the number of dendritic beads and L is the number of linear beads. W[13−15] is, for any branched

* To whom correspondence should be addressed. E-mail: t.mulder@tue.nl.

10.1021/ma049612k CCC: $30.25 © 2005 American Chemical Society
Published on Web 01/11/2005

N-beads structure, defined as

$$W = \frac{1}{2}\sum_{i,j=1}^{N} d_{ij} \tag{2}$$

where d_{ij} is the number of monomer segments separating beads i and j. Lyulin et al.[16] demonstrated typical dendrimer behavior for the viscosity of HBPs with high values of DB. Both the Monte Carlo study of Widmann and Davies[12] and the Brownian dynamics study of Sheridan et al.[17] demonstrated scaling behavior of the intrinsic viscosity with the molecular weight and with W. Sheridan et al. also found a power-law relation connecting the radius of gyration of an HBP to its W value. Geladé et al.[18] used small-angle neutron scattering combined with other techniques for structural characterization of hyperbranched polyesteramides: the fractal dimensions that are measured could be explained from theory on randomly branched polymers. Mendoza and Marques[19] demonstrated the influence of polydispersity and nature of the branching on the scattering structure factor in the intermediate wave-vector regime. The use of AB monomers in the synthesis process besides the usual AB_2 monomers was investigated by Aerts[20] and Lee et al.[21]

The goal of the present paper is to contribute to clarifying the conformational behavior of HBPs, in particular to study the influence of perturbations of the regular dendrimer topology on its configurations. To that end, Brownian dynamics simulations have been performed of HBPs that, via the topological parameters DB and W, are classified on the basis of their difference with pure dendrimers. Comparisons have been made between simulated HBPs and dendrimers in total size and in internal mass distribution. The total size has also been estimated from mean-field calculations. For that purpose the mean-field theory developed by Evers et al.[3] for dendrimers has been generalized to HBPs. In particular, HBPs with charged end groups have been simulated. An electrostatic contribution to the single-HBP Helmholtz free energy has been derived to perform mean-field calculations on these structures.

The remainder of the article starts with a description of the (model) structures that are investigated and of the simulation method. In section 3 the Helmholtz free energy expressions are derived. The results of the simulations are presented and compared to the predictions of the mean-field theory in section 4. The conclusions are presented in section 5.

2. Model and Simulation Algorithm for Hyperbranched Polymers

A HBP in a solution is simulated by using the Brownian dynamics simulation method.[22] The HBP is represented by beads (for the monomers) connected by rigid rods of length l; the (fast-moving) solvent particles are not explicitly simulated, and they are replaced by a continuum which exerts a friction force and a random force of the same magnitude on the beads. This continuum is further characterized by a temperature T, friction coefficient ζ, a Bjerrum length λ_B, and a Debye length κ^{-1}.

Figure 1 shows the bead−rod representations of two model HBPs. There are no restrictions on the angle between two adjacent rods. Monomers of the same generation are depicted on one dashed circle. The structures of Figure 1, labeled with type 1 and type 2, represent two different categories of HBPs. The structure of type 1 belongs to the category of HBPs with all terminal groups in the same generation. Type 2 structures are HBPs of which the terminal groups are distributed over all generations. This distinction is essential for a description of the structures in a mean-field theory. Both structures have been simulated in the present work.

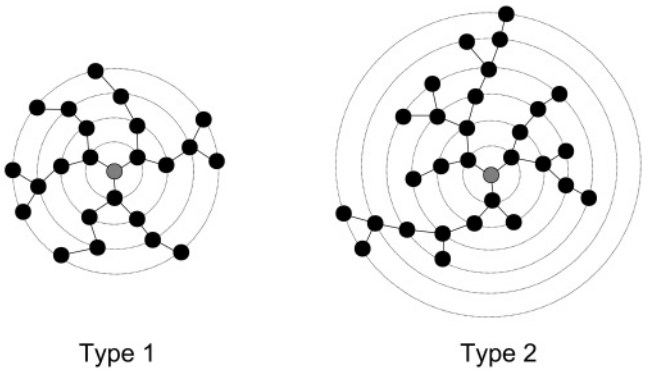

Figure 1. Bead−rod representations of two HBPs. The beads, which represent the monomers, are separated by rigid rods of length l. Monomers of the same generation are depicted on one dashed circle. The structure labeled with type 1 represents the category of HBPs with all terminal groups in the same generation; the structure labeled with type 2 represents the category of HBPs with the terminal groups distributed over all generations.

A model HBP consisting of N beads is built of one core bead surrounded by $(N - 1)$ internal beads. The core has a functionality f_{core}, and the internal beads have a functionality f. These internal beads are distributed over g_{max} generations. The core bead and the beads of generation g are separated by g rods of length l. The HBPs considered in this study have functionalities $f_{core} = 3$ and $f = 3$. The degree of branching DB is given by

$$DB = \frac{N_B}{N_{B,max}} \tag{3}$$

in which N_B is the actual number of branching points and $N_{B,max}$ the maximum number of branching points at fixed value of N. This maximum number of branching points, which equals the number of branching points in a dendrimer (with $f_{core} = 3$ and $f = 3$), is given by

$$N_{B,max} = N/2 - 1 \tag{4}$$

This definition for the degree of branching is equivalent to the definition of Widmann and Davies.[12] The number of end groups, or functional groups, N_T, is given by

$$N_T = 2 + DBN_{B,max} = 2 + DB(N/2 - 1) \tag{5}$$

The synthesis of type 1 structures, although we do not know whether they have been synthesized in real life already, is based on the (divergent) synthesis of dendrimers (see the paper Bosman et al.[7] and references therein): the idea is that the structures are grown generation by generation, but instead of adding one type of monomer, two types of monomers are added. As a first step in the procedure to build a N-beads structure with a degree of branching DB, a core bead is placed in the center of a reference frame. In the next step three beads are attached onto the core. The result is a generation $g = 1$ dendrimer. Onto every bead of generation $g = 1$

one or two beads are attached, resulting in a HBP of generation $g = 2$. This attaching process is highly dependent on the value of P_{linear}, which is the probability that a monomer in a generation $(g - 1)$ is of type AB (the B group can be attached to an A group of a monomer in the next generation), so that only one generation g monomer can be attached. The probability that a monomer in generation $(g - 1)$ is of type AB_2 (both B groups can be attached to an A group of a monomer in the next generation), so that two generation g monomers can be attached, equals $(1 - P_{\text{linear}})$. The *DB* of the final structure is determined by P_{linear}. From the input value of *DB* the algorithm calculates the value of P_{linear} necessary to create a structure with this prescribed degree of branching. This process is repeated until all N beads have been attached, resulting in an HBP of generation $g = g_{\max}$. An alternative method to create type 1 HBPs might be following a dendrimer-like synthesis process, using monomers of different lengths. Type 2 HBPs are built of AB_2 monomers. The building procedure, described into detail by Widmann and Davies,[12] of a type 2 HBP of N beads again starts by placing a core in the center of a reference frame. The monomers are attached one by one to free groups of the structure. The *DB* of the final structures is dependent on the reaction probabilities of the free groups.[25] A comparable building procedure was used by Aerts.[20] These synthetic procedures do not resemble the real AB_2 polycondensation process. However, they can be used to create hyperbranched structures that can be characterized by topological parameters (N and $g_{\max}$ in case of type 1 HBPs and N and *DB* in case of type 2), which influence on the conformational behavior is investigated in this paper.

All nonbonded beads interact via a Lennard-Jones potential

$$U_{\text{LJ}}(r) = \begin{cases} 4\epsilon_{\text{LJ}}\left(\left(\frac{\sigma}{r}\right)^{12} - \left(\frac{\sigma}{r}\right)^{6}\right) - U_{\text{LJ}}^{\text{c}} & r < r_{\text{c}} \\ 0 & r > r_{\text{c}} \end{cases} \quad (6)$$

in which $\sigma = 0.8l$, $\epsilon_{\text{LJ}} = 0.3k_{\text{B}}T$ and $r_{\text{c}} = 2l$. These values were used by de la Torre and co-workers[24] to correctly reproduce the molecular weight dependence of the average square end-to-end distance, $\langle R^2 \rangle$, of a linear chain in a Θ-solvent. The initial positions of the beads are chosen such that the distance between the bead that is added and all the previously added beads is restricted to be larger than 0.8σ ($0.64l$) to avoid strong repulsion of the beads. All terminal beads are charged and interact via the Debye−Hückel potential:

$$\frac{U_{\text{C}}(r)}{k_{\text{B}}T} = z^2\lambda_{\text{B}}\frac{\exp(-\kappa r)}{r} \quad (7)$$

z is the effective charge of the end groups, λ_{B} is the Bjerrum length, and κ is the inverse Debye length, which describes the screening of the electrostatic interactions due to the presence of counterions and salt in the solution.

In the simulation the positions of the monomers are calculated after every time step Δt employing the Ermak−McCammon equation.[23] In this algorithm the influence of the solvent particles on the monomers is accounted for by incorporating a dissipative force, due to the friction of the diffusing monomer with the average solvent, and a fluctuating force, due to the random collisions of the monomer with the solvent particles. Details of the simulation algorithm are described by Evers et al.[3]

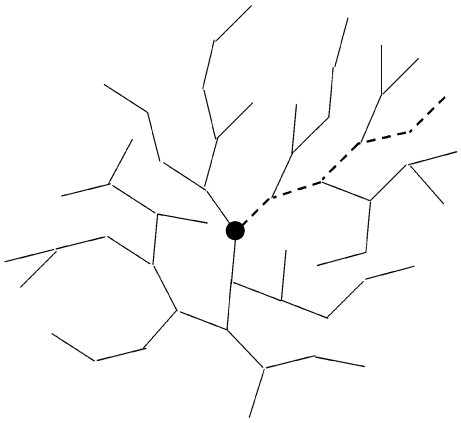

Figure 2. Single path of monomers (dashed line), connecting the core (the sphere) to an end group.

Type 1 HBPs with N up to 382 monomers and with *DB* varying from 0 (linear structures) to 1 (perfect dendrimers), and type 2 HBPs with $N = 94$ and *DB* between 0 and 1, have been simulated. For the various combinations we produce one realization, which is used in the Brownian dynamics simulation. HBPs with excluded-volume interactions only, HBPs with Coulomb interactions only, and HBPs with both excluded-volume and Coulomb interactions have been simulated. For the Coulomb interactions an effective charge of $z^2 = 1$ has been used; for the Bjerrum length and the Debye screening length the values $\lambda_{\text{B}} = l$ and $\kappa^{-1} = 100l$ have been used, respectively.

A dimensionless time step $\Delta t = 1 \times 10^{-4}$ is chosen in all simulations, which results in a maximum bead displacement of less than 5% of the bond length l. All simulations start with the relaxation of the simulated system until the gyration radius of the HBP fluctuates around its average value ($R_g \pm \sigma_{R_g}$), where the fluctuations are typically smaller than 10% of the average value ($\sigma_{R_g} \leq 0.1R_g$). The number of time steps necessary for the relaxation varies from 2.5×10^5 for systems with $N = 10$ beads to 2.0×10^6 for systems with $N = 382$ beads. After equilibration, the simulation is proceeded for between 5.0×10^5 and 1.25×10^6 production time steps, during which statistical properties of the simulated system are calculated.

For each simulated hyperbranched structure, the radius of gyration, the distribution of monomers over shells that are concentric with the core monomer of the HBP, and the structure factor have been calculated.

3. Mean-Field Theories for Neutral and Charged HBPs

3.1. Uncharged (Dendrimers and) HBPs of Type 1. The free energy of a single path of monomers, from the core to any end group, in a neutral dendrimer of generation g (see Figure 2) may be written as[2]

$$\frac{F}{k_{\text{B}}T} = \frac{\Delta F_{\text{el}}}{k_{\text{B}}T} + \frac{\Delta F_{\text{conf}}}{k_{\text{B}}T} + g\phi = \frac{3}{2}\alpha^2 - 3\ln\alpha + g\phi_0\alpha^{-3} \quad (8)$$

in which k_{B} is Boltzmann's constant, T the temperature, ϕ the mean monomer density, and α the linear expansion factor. The first term gives the entropic contribution

to the free energy due to stretching of the path of monomers. It is assumed that the path of monomers is not strongly stretched but exhibits Gaussian statistics. The entropic free energy contribution due to compression is represented by the second term. The third term accounts for the excluded-volume interactions of the monomers of the path with the other monomers. Only two-body interactions are taken into account. $\alpha = (R_g/R_{g0})$, where R_g is the average radius of gyration of the structure and R_{g0} the average radius of gyration of the same structure without any interactions between nonbonded beads (ideal structures). Since the structures in this study are built of freely jointed particles, the gyration radius R_{g0} is related to the Wiener index W as follows:[13,14]

$$R_{g0}^{\ 2} = \frac{Wl^2}{N^2} \tag{9}$$

The mean monomer density ϕ is given by

$$\phi = \frac{Nv}{R_g^{\ 3}} = \frac{Nv}{R_{g0}^{\ 3}}\alpha^{-3} = \phi_0\alpha^{-3} \tag{10}$$

where v is the excluded-volume parameter (a fitting parameter that gives the strength of the excluded-volume interactions) and ϕ_0 the mean monomer density of ideal dendrimers.

Evers et al.[3] included three- and higher-body virial coefficients in the excluded-volume term using a free volume type of approach: the excluded-volume term is then written as $-g\ \ln(1 - \phi)$. To account for van der Waals attraction, a term $-g\phi\epsilon$ is added, in which ϵ is a fitting parameter that gives the strength of the attraction. The final free energy can then be written as

$$\frac{F}{k_BT} = \frac{\Delta F_{el}}{k_BT} + \frac{\Delta F_{conf}}{k_BT} + \frac{\Delta F_{vdW}}{k_BT} \tag{11}$$

in which

$$\frac{\Delta F_{vdW}}{k_BT} = -g\ \ln(1 - \phi) - g\phi\epsilon \tag{12}$$

Equations 8−12 are also valid for HBPs of type 1. However, it should be noted that whereas for dendrimers the generation is a function of the number of monomers only ($g = g(N)$); for HBPs the generation is also dependent on the Wiener index ($g = g(N,W)$). The equilibrium size of the dendrimer in terms of α can be found by minimizing the free energy. To be able to calculate R_g ($= \alpha R_{g0}$) for any number of generations g, $R_{g0}(g)$ has to be determined. This is done in Appendix A.

3.2. Uncharged HBPs of Type 2. For type 2 HBPs the end groups are distributed over all generations; i.e., there is a distribution of the path lengths l_p. This path length distribution $T(l_p)$ is approximated by a Gaussian distribution:

$$T(l_p) = \frac{N_T}{\sigma_g\sqrt{2\pi}}\exp\left(-\frac{1}{2}\left(\frac{l_p - \langle g\rangle}{\sigma_g}\right)^2\right) \tag{13}$$

$\langle g\rangle$ is the mean generation number, defined as the mean number of monomers separating an end group from the core, and σ_g is the standard deviation. $\langle g\rangle$ and σ_g are somehow related to the degree of branching. To determine these parameters for HBPs with a degree of branching *DB* within a certain range, 10 HBPs are created with a degree of branching *DB* within this range according to the procedure described in section 2. Subsequently, the average end group distribution of these HBPs is calculated and fitted by a Gaussian. Table 1 contains the values of the fit parameters $\langle g\rangle$ and σ_g for various ranges of *DB* for HBPs with $N = 94$, together with information on the actual distributions. Two type 2 HBPs and their end group distributions are shown in Figure 3. As can be seen, $\langle g\rangle$ and σ_g decrease when *DB* increases.

Table 1. Fit Parameters $\langle g\rangle$ and σ_g for Various Ranges of *DB* for HBPs with $N = 94$, Together with Information on the Actual Distributions

N, *DB*	$\langle g\rangle$	σ_g	av	std dev	skewness	kurtosis
94, 0.40−0.60	8.5 ± 0.3	5 ± 2	8.5	2.9	0.1	2.3
94, 0.60−0.75	6.9 ± 0.2	2.4 ± 0.3	7.0	2.2	0.1	2.8
94, 0.75−0.85	6.1 ± 0.1	1.8 ± 0.1	6.3	1.9	0.4	3.1
94, 0.85−0.95	6.0 ± 0.1	1.6 ± 0.1	6.1	1.8	0.4	3.6
94, 0.95−1.00	6.1 ± 0.1	1.8 ± 0.1	6.2	1.9	0.2	3.0

Equations 8−12 can be generalized for any path of monomers connecting an end group to the core in type 2 HBPs by replacing g by l_p. To obtain an approximation for the expansion factor of a type 2 HBP, the free energy of a path of length $l_p = \langle g\rangle$ is minimized. $\langle g\rangle$ is dependent on the position of the core monomer, which should be chosen such that variation in length of the different branches is as small as possible. The smaller this variation is, the more reliable is the expansion factor α, calculated for one branch, as a measure for the overall expansion of the whole HBP. The synthetic core that is used in the calculations in this paper reasonably fulfills this requirement. For the calculation of R_g, R_{g0} is calculated for all type 2 structures that are studied, either by mean-field calculations or by simulation.

3.3. Type 1 HBPs with Charged End Groups. For dendrimers with charged end groups Evers et al.[3] derived the following expression for the free energy:

$$\frac{F}{k_BT} = \frac{\Delta F_{el}}{k_BT} + \frac{\Delta F_{stretch}}{k_BT} + \frac{\Delta F_{conf}}{k_BT} + \frac{\Delta F_{Q/1}}{k_BT} \tag{14}$$

in which

$$\frac{\Delta F_{stretch}}{k_BT} = -\frac{9}{20}\frac{1}{\sqrt{g}}\alpha^3\ln\left(1 - \frac{\alpha}{\sqrt{g}}\right) \tag{15}$$

and

$$\frac{\Delta F_{Q/1}}{k_BT} = z^2\lambda_B\frac{N_T}{R_{g0}}\frac{1}{\alpha} \tag{16}$$

Assuming that the branches are strongly stretched due to electrostatic interactions (of the end groups), the first two terms of eq 14 have been introduced to replace the first term of eq 11. The third term is equivalent to the second term of eq 8. The last term accounts for the electrostatic interactions, on the condition that the Debye length is large in comparison to the outer radius R of the dendrimer ($\kappa^{-1} \gg R$). Excluded-volume terms are left out.

Equation 14 should also be valid for HBPs of type 1. Yet, for these charged HBPs, it is not possible to find a

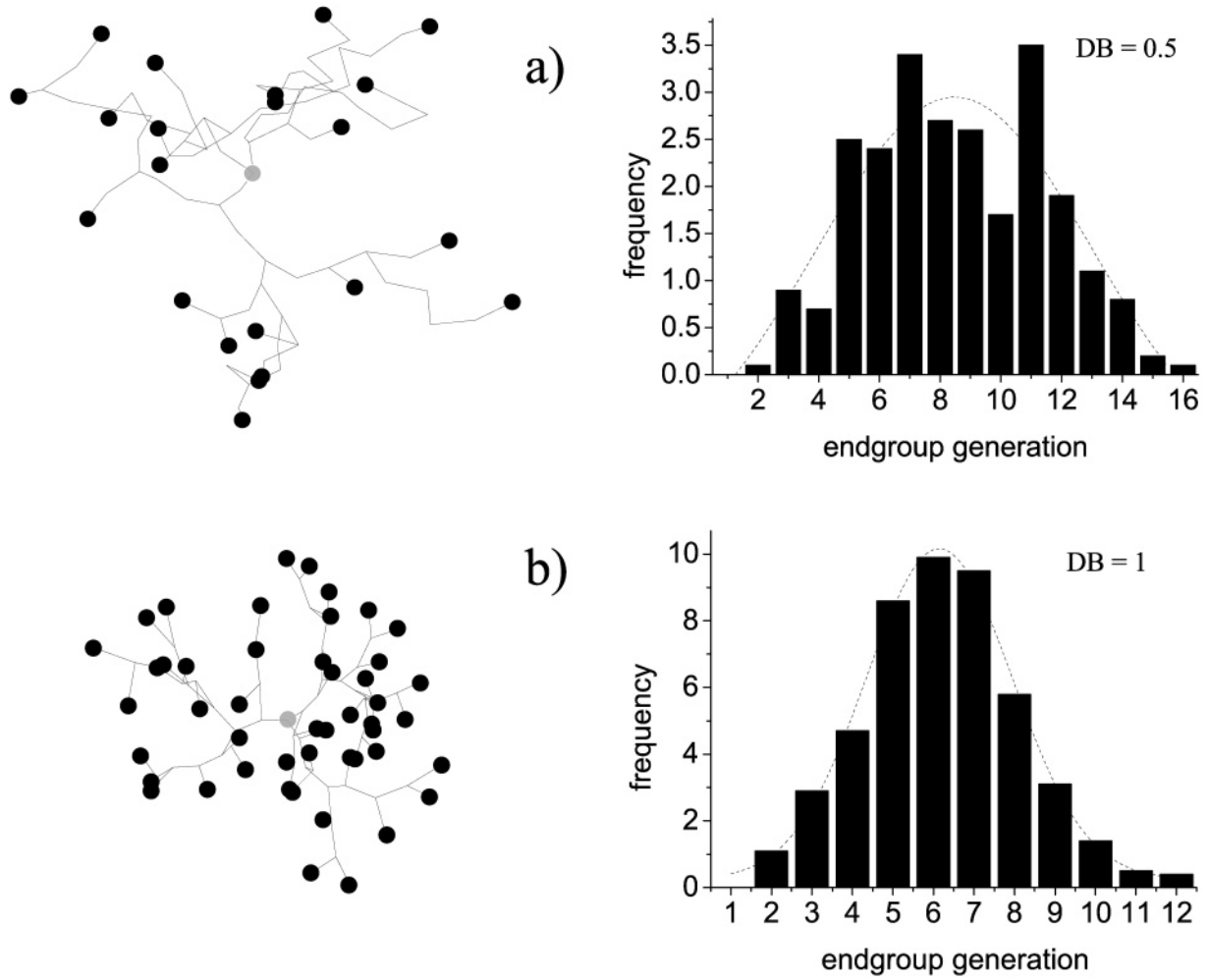

Figure 3. Distribution of path lengths for type 2 HBPs with (a) $DB = 0.5$ and (b) with $DB = 1$. (Both HBPs are schematically depicted in the left part of this figure: the black spheres represent end groups, and the gray sphere represents the core.) These path length distributions can be approximated by a normal distribution with a mean value $\langle g \rangle$ and a standard deviation σ_g. For the HBP with $DB = 0.5$ $\langle g \rangle = 8.5 \pm 0.3$ and $\sigma_g = 5 \pm 2$; for the HBP with $DB = 1$ $\langle g \rangle = 6.1 \pm 0.1$ and $\sigma_g = 1.8 \pm 0.1$.

one-to-one relation between gyration radius R_g and the number of generations g. The topological variety among the structures that belong to a collection of HBPs for which N and g are fixed results in a variety of the number of terminal groups N_T: for any HBP with fixed N and g the number of end groups can vary between some minimal value and some maximal value, resulting in an expansion factor between some minimal value and some maximal value, respectively. This will be further discussed below.

If excluded-volume interactions are incorporated, eq 14 becomes

$$\frac{F}{k_B T} = \frac{\Delta F_{el}}{k_B T} + \frac{\Delta F_{stretch}}{k_B T} + \frac{\Delta F_{conf}}{k_B T} + \frac{\Delta F_{vdW}}{k_B T} + \frac{\Delta F_{Q/1}}{k_B T} \quad (17)$$

3.4. Type 2 HBPs with Charged Free B Groups. As for type 1 HBPs, it is assumed that the different branches within charged type 2 HBPs are strongly stretched. The only difference of a branch of a type 2 HBP with a branch of a type 1 HBP is that the charged groups are located in another charge distribution. So eqs 14−17 are generalized for any path of monomers connecting an end group to the core of a type 2 HBP by replacing g by l_p and by recalculating the free energy contribution of the electrostatic interactions.

The distribution of the free B groups is approximated by a spherically symmetric Gaussian distribution. The charge density can therefore be approximated by

$$\rho(r) = \frac{zN_T}{\sigma_c\sqrt{2\pi}} \frac{\exp\left(-\frac{1}{2}\left(\frac{r-\mu_c}{\sigma_c}\right)^2\right)}{4\pi r^2} \quad (18)$$

in which r is the distance to the core monomer, μ_c is the average distance of the free B groups to the core, and σ_c is the standard deviation of the free B group distribution. The electrostatic interactions of the charges on a path of monomers result in a free energy contribution $\Delta F_{Q/2} = \Delta F_{Q/2}(r'_1, ..., r'_n, \mu, \sigma)$, in which $\vec{r}'_1, ..., \vec{r}'_n$ are the positions of the charges with respect to the core, which is derived in Appendix B.

To calculate the expansion factor α of a charged type 2 HBP, its free energy is minimized for a path of $l_p = \langle g \rangle$ monomers. For such a path of monomers $r'_i \simeq \alpha\sqrt{i \,/\, n\langle g \rangle}$, $i = 1, ..., n$, $\mu_c \simeq \alpha\sqrt{\langle B \rangle}$, and $\sigma_c \simeq \alpha\sqrt{\sigma_B}$, with $\langle B \rangle$ the average number of monomer segments separating a free B group from the core and σ_B the standard deviation of B. The values of $\langle B \rangle$ and σ_B are determined in the same way as $\langle g \rangle$ and σ_g were determined in section 3.2. The results are given in Table 2.

Table 2. Fit Parameters $\langle B\rangle$ and σ_B for Various Ranges of *DB* for HBPs with $N = 94$, Together with Information on the Actual Distributions

N, *DB*	$\langle B\rangle$	σ_B	av	std dev	skewness	kurtosis
94, 0.40−0.60	7.3 ± 0.2	3.8 ± 0.4	7.5	3.0	0.2	2.3
94, 0.60−0.75	6.4 ± 0.1	2.5 ± 0.2	6.5	2.2	0.2	2.7
94, 0.75−0.85	6.0 ± 0.1	1.7 ± 0.1	6.1	1.9	0.4	3.1
94, 0.85−0.95	6.0 ± 0.1	1.6 ± 0.1	6.1	1.8	0.4	3.6
94, 0.95−1.00	6.1 ± 0.0	1.8 ± 0.1	6.2	1.9	0.2	3.0

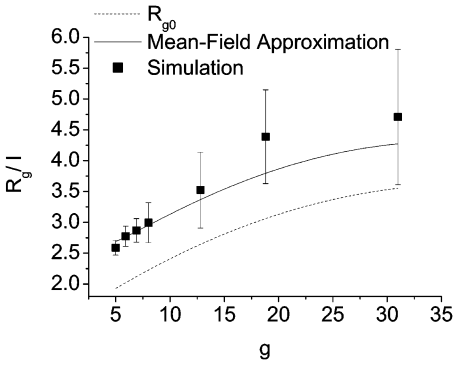

Figure 4. Radius of gyration as a function of the number of generations for uncharged type 1 HBPs of $N = 94$ beads with excluded-volume interactions. The values of R_g following from the simulations are compared to the predictions of the mean-field theory. The values of the radii of gyration R_{g0} for ideal structures are also plotted.

4. Simulation Results and Comparison with Mean-Field Approximations

4.1. Gyration Radius of Uncharged Type 1 HBPs. In Figure 4 the gyration radii that have been found in the simulation of uncharged type 1 HBPs of $N = 94$ monomers (with excluded-volume interactions) have been plotted, together with the results of the mean-field calculations (derived in section 3.1). The bars represent the statistical errors of the simulation, which increase with increasing g. In the mean-field calculations for the adjustable parameters the values $v = (\sigma/2)^3 = 0.064l^3$ and $\epsilon = 0.3$ are used. The radii of gyration of the ideal structures R_{g0} have also been plotted.

The structure with the minimum number of generations ($g = 5$) is a dendrimer. An increase in the number of generations immediately results in an increase of the gyration radius, despite N being constant. For HBPs with a small number of generations (a few more generations than the dendrimer with the same number of beads) the results of the Brownian dynamics simulations are in good agreement with the predictions of the mean-field calculations. For HBPs with higher values of g the mean-field calculation slightly underestimates the values of the gyration radii that follow from the simulations. This may be attributed to the fact that the attractive interactions between the monomers of HBPs are represented by a term that is proportional to the monomer density, i.e., proportional to the number of beads in some active range around any monomer. (The interaction of the monomer with monomers outside its active range is negligible.) Such a representation would be correct only if the monomer−monomer interaction potential were constant in this active range. For the Lennard-Jones potential of the present study this shortcoming results in an overestimation of the attractive interactions in the mean-field approximation, which leads to the underestimation of the gyration radii as the number of generations increases. HBPs with a different number of monomers show the same qualitative behavior.

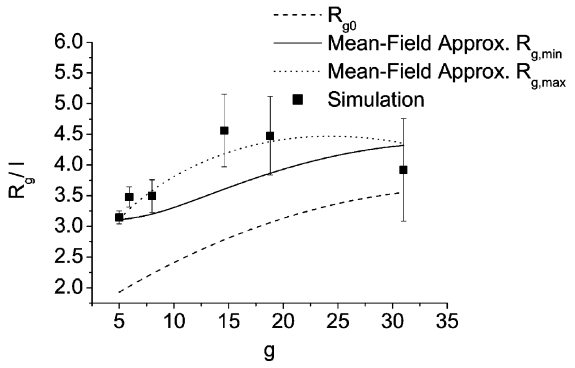

Figure 5. Gyration radii of type 1 HBPs of $N = 94$ beads with both excluded-volume interactions and Coulomb interactions ($z^2 = 1$) following from the simulations are compared to the mean-field predictions. The gyration radii R_{g0} of the ideal structure are also given.

4.2. Gyration Radius of Charged Type 1 HBPs. Figure 5 shows both the radii of gyration of charged type 1 HBPs that follow from the mean-field calculations and those that follow from the simulations, together with the minimal value of the gyration radius $R_{g,\min}$ and the maximal value of the gyration radius $R_{g,\max}$ (corresponding to the minimal and the maximal number of end groups, respectively) calculated using the mean-field approximations. The gyration radii of the ideal type 1 HBPs are also given.

The simulation results are in reasonable agreement with the mean-field calculations. However, one should realize that the mean-field theory has its shortcomings: apart from the problem with the density as discussed in section 4.1, there is the fact that the branches of the HBP are not fully stretched ($\alpha < \sqrt{g}$), which means that the contribution $\Delta F_{\text{stretch}}$ to the free energy is not fully justified. HBPs with a different number of monomers show the same qualitative behavior.

4.3. Gyration Radii of Type 2 HBPs. To obtain an approximation of the swelling of a type 2 HBP, the free energy has been minimized for a path of length $l_p = \langle g\rangle$ (see section 3.2). This has been done for 10 different (uncharged and charged) structures per range of *DB* values as given in Table 1. The resulting values for the gyration radii are plotted both vs $\langle g\rangle$ and vs *DB* in Figure 6. The gyration radii of the ideal counterparts are also given. For the adjustable parameters $v = (\sigma/2)^3 = 0.064l^3$, $\epsilon = 0.3$ and $z^2 = 1$ are used. Both for the uncharged HBPs and for the charged HBPs the predictions of the mean-field approximations are in good agreement with the simulation results. Note that for the charged HBPs $\alpha \approx \sqrt{g}$, so that the contribution $\Delta F_{\text{stretch}}$ to the free energy is correct. For the uncharged type 2 HBPs R_g is hardly sensitive to variation of *DB*, whereas for charged structures R_g is a decreasing function of *DB*.

4.4. Wiener Index Dependence of the Gyration Radius for Uncharged HBPs with Excluded-Volume Interactions. Sheridan et al.[17] report, for simulated freely jointed HBPs with exactly the same excluded-volume interactions as used in the present simulations, the following scaling law:

$$R_g^2 \propto W^a N^{-b} \tag{19}$$

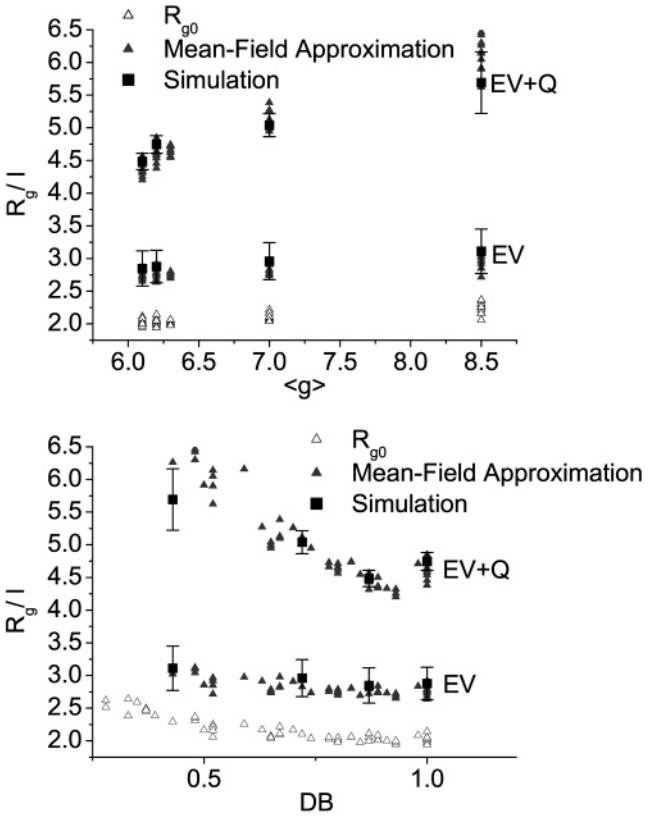

Figure 6. Radius of gyration both as a function of the average number of generations $\langle g \rangle$ and as a function of *DB* for type 2 HBPs of $N = 94$ monomers with only excluded-volume interactions (EV) and for type 2 HBPs with both excluded-volume and Coulomb ($z^2 = 1$) interactions (EV + Q). The results of the simulations and the mean-field calculations are in good agreement. The gyration radii of the ideal HBPs are also plotted.

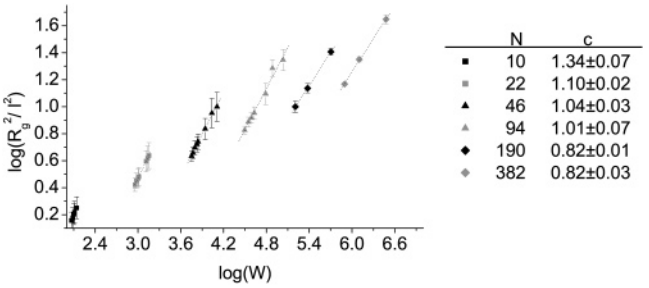

Figure 7. Radius of gyration as a function of the Wiener index for uncharged type 1 HBPs with excluded-volume interactions. Note that $R_g \propto W^c$, where c depends on the number of monomers N. This contrasts the findings of Sheridan et al.,[17] who report $c = 1$, independent of N.

in which $a = 1$ and $b = 1.7$. These values change as the parameters of the excluded-volume interactions (ϵ and σ) are altered. To compare with the present study, we write for our data

$$R_g{}^2 \propto W^c N^{-d} \tag{20}$$

$c = c(N)$ is given in Figure 7 for various values of N. From the plot of $\ln((R_g{}^2/W^c))$ vs $\ln(N)$ it follows that the value of the exponent is $d = 1.7$, in agreement with ref 17. In Figure 7 results on type 1 HBPs are used to determine the scaling law $R_g{}^2 \propto W^c$. Type 2 structures were not used, as the amount of simulation data was quite restricted.

Remarkably, as N increases, the dependence of the gyration radius R_g on W gets weaker; i.e., $c(N)$ decreases, in contrast to the findings of Sheridan et al. Since the difference between Sheridan's structures and the type 1 HBPs of this paper is in the architecture, this dependence of c on N indicates that the relation between size and architecture of hyperbranched polymers with excluded-volume interactions is not given by a simple scaling law between $R_g{}^2$ and W. At best there might be a scaling within regions of the whole phase space. The scaling exponent reported by Sheridan, which is based on a huge amount of data (that covers a large part of the phase space), is probably some average of the scaling exponents that are found for the different regions in phase space.

For charged structures no scaling law of the form (20) is found. The size of charged structures is mainly determined by the strength of the Coulomb interactions.

4.5. Radial Mass Distributions. To obtain a clear picture of how structural irregularities influence the way monomers of an HBP are distributed in space, the radial mass distributions of the simulated HBPs are studied. The radial mass distribution $m(r/l)$ is defined as

$$m(r/l\ ) = \frac{\mathrm{d}\langle n(r/l)\rangle}{\mathrm{d}(r/l)} \tag{21}$$

where $\langle n(r/l)\rangle$ is the time-averaged number of beads within a sphere of radius (r/l) that is centered at the core monomer. As a consequence

$$\int_0^{R/l} m(r/l)\ \mathrm{d}(r/l) = N \tag{22}$$

in which R is the outer radius of a sphere enclosing the whole HBP and N is the total number of monomers. The radial mass distributions $m_g(r/l)$ of the monomers belonging to one generation g (or a few subsequent generations) are defined as

$$m_g(r/l) = \frac{\mathrm{d}\langle n_g(r/l)\rangle}{\mathrm{d}(r/l)} \tag{23}$$

in which $\langle n_g(r/l)\rangle$ is the average number of generation-g monomers within a sphere of radius (r/l) that is centered at the core monomer. Then

$$\sum_{g=0}^{g_{\max}} \int_0^{R/l} m_g(r/l)\ \mathrm{d}(r/l) = \sum_{g=0}^{g_{\max}} N_g = N \tag{24}$$

in which N_g is the number of monomers in one generation.

In Figure 8 the mass distributions are given of (a) an uncharged type 1 HBP (with excluded-volume interactions) of $N = 94$ monomers and $g_{\max} = 6$ generations ($DB = 0.87$), (b) a charged type 1 HBP (with both excluded-volume and Coulomb ($z^2 = 1$) interactions) with $N = 94$ and $g_{\max} = 6$ ($DB = 0.87$), and (c) a charged type 1 HBP (with both excluded-volume and Coulomb ($z^2 = 1$) interactions) with $N = 94$ and $g_{\max} = 9$ ($DB = 0.50$). The distributions $m_g(r/l)$ for different values of g in the uncharged HBP show much spatial overlap. Charging the end groups results in an internal ordering: monomers from the same generation arrange in concentric shells around the core (compare parts a and b of Figure 8). This effect is most pronounced for

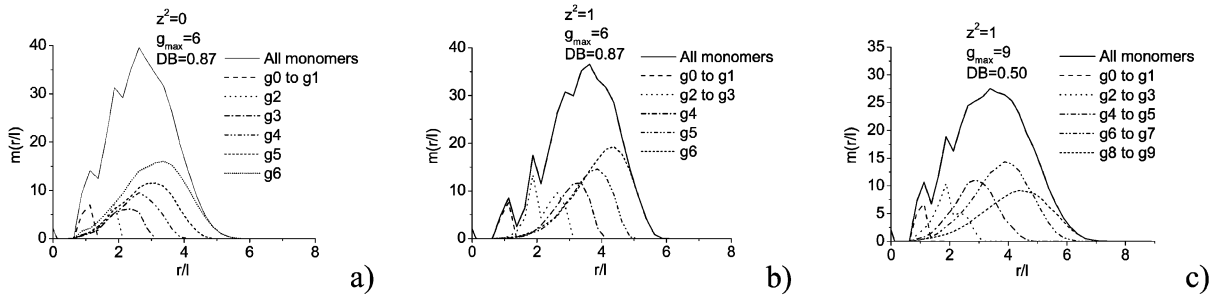

Figure 8. Radial mass distributions of (a) an uncharged type 1 HBP (with excluded-volume interactions) of $N = 94$ monomers and $g_{max} = 6$ generations ($DB = 0.87$), (b) a charged type 1 HBP (with both excluded-volume and Coulomb ($z^2 = 1$) interactions) with $N = 94$ and $g_{max} = 6$ ($DB = 0.87$), and (c) a charged type 1 HBP (with both excluded-volume and Coulomb ($z^2 = 1$) interactions) with $N = 94$ and $g_{max} = 9$ ($DB = 0.50$). The distributions $m_g(r/l)$ of the uncharged HBP show much spatial overlap. In charged type 1 HBPs the monomers of the same generation arrange into concentric shells around the core (compare parts a and b). This ordering effect is most pronounced for dendrimers ($g_{max} = 5$). An increase of the number of generations g_{max} (decrease of the degree of branching) results in more overlap of the distributions $m_g(r/l)$ (compare parts a and c).

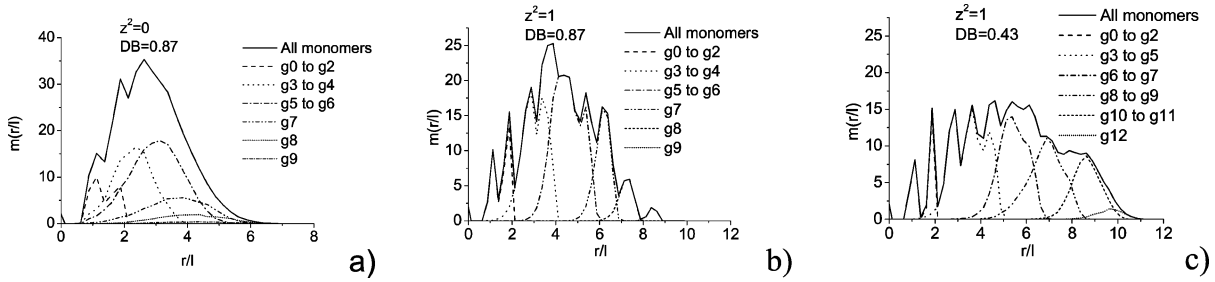

Figure 9. Radial mass distributions of (a) an uncharged type 2 HBP (with excluded-volume interactions) with $N = 94$ and $DB = 0.87$, (b) a charged type 2 HBP (with both excluded-volume and Coulomb ($z^2 = 1$) interactions) with $N = 94$ and $DB = 0.87$, and (c) a charged type 2 HBP (with both excluded-volume and Coulomb ($z^2 = 1$) interactions) with $N = 94$ and $DB = 0.43$. Charging the end groups results in an internal ordering: monomers from the same generation arrange in concentric shells around the core (compare parts a and b). The ordering is stronger than for type 1 HBPs, and it is maintained as the degree of branching is lowered, although less so for $DB = 0.43$ (compare parts b and c).

dendrimers ($g_{max} = 5$). An increase of the number of generations g_{max} (decrease of the degree of branching) results in more overlap of the distributions $m_g(r/l)$ (compare parts b and c of Figure 8). At $g_{max} \approx 10$ ($DB \approx 0.5$) the ordering has almost vanished. This ordering effect becomes stronger as the effective charge z^2 is increased. The influence of the number of monomers of the HBP on the internal ordering has also been studied. For HBPs with the same values of DB and z^2 a change in the value of N does not significantly change the ordering of the monomers.

The influences of the valence, the degree of branching, and the number of monomers on the internal ordering can be understood from the fact that these parameters directly influence the Coulombic interactions. The Coulombic term in the Helmholtz free energy is directly proportional to z^2 and to the number of end groups N_T (and therefore, according to eq 5, to a good approximation proportional to DB and N). Changing DB or N also influences the size of the HBP. An increase in DB results in a decrease in size (and with it a decrease in the distances between the charges of the HBP), which reinforces the effect of a larger number of terminal groups. An increase in N results in an increase in size, which inhibits the effect of a larger number of terminal groups. As a consequence, the dependence of the internal ordering on N is weaker than its dependence on λ_B and DB.

The radial mass distributions of (a) an uncharged type 2 HBP (with excluded-volume interactions) with $N = 94$ and $DB = 0.87$, (b) a charged type 2 HBP (with both excluded-volume and Coulomb ($z^2 = 1$) interactions) with $N = 94$ and $DB = 0.87$, and (c) a charged type 2 HBP (with both excluded-volume and Coulomb ($z^2 = 1$) interactions) with $N = 94$ and $DB = 0.43$ are given in Figure 9. Charging the end groups again results in an internal ordering: monomers from the same generation arrange in concentric shells around the core (compare parts a and b of Figure 9). The ordering is stronger than for type 1 HBPs, and it is maintained as the degree of branching is lowered, although less so for $DB = 0.43$ (compare parts b and c of Figure 9).

4.6. Static Structure Factor. All structural properties of HBPs presented above can be measured in small-angle scattering experiments. The scattered radiation intensity that is studied in these experiments is proportional to the static structure factor

$$S(q) = \frac{1}{N^2}\left\langle \sum_{n=1}^{N}\sum_{m=1}^{N} \exp(i\vec{q}\cdot(\vec{r}_n - \vec{r}_m)) \right\rangle \qquad (25)$$

which can be calculated from the present simulations. Here $\vec{q}$ is the scattered radiation vector, defined as

$$q = |\vec{q}| = \frac{4\pi}{\lambda}\sin(\Theta/2) \qquad (26)$$

Θ is the scattering angle, λ is the wavelength, and $\vec{r}_n$ are the coordinates of the scattering centers.

In parts a and b of Figure 10 the calculated static structure factors are given of type 2 HBPs of $N = 94$ monomers, with only excluded-volume interactions and with both excluded-volume and Coulomb ($z^2 = 1$) interactions, respectively. The two figures show a marked difference between uncharged and charged HBPs: for the latter the structure factors contain

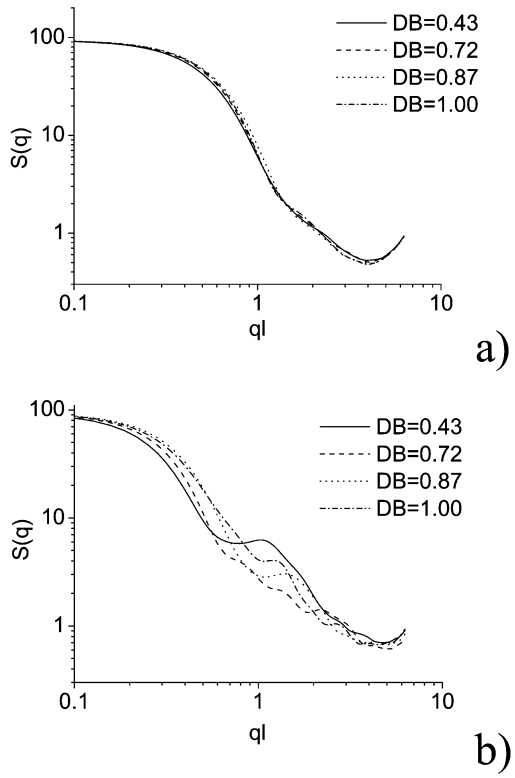

Figure 10. (a) Static structure factors of type 2 HBPs of $N = 94$ monomers with (a) excluded-volume interactions and (b) excluded-volume and Coulomb ($z^2 = 1$) interactions. The degree of branching varies from $DB = 0.43$ to $DB = 1.00$. The structure factors of the HBPs with Coulomb interactions show oscillations which are related to the internal ordering (separation of generations, see Figure 6).

oscillations (especially for high degrees of branching *DB*), which are related to the ordering (separation of generations) observed earlier. These oscillations vanish as soon as the mass distribution becomes smooth. The static structure factors of charged type 1 HBPs exhibit the same behavior.

5. Conclusions

In this investigation Brownian dynamics simulations have been performed for two types of HBPs, type 1 and type 2. HBPs of type 1 have all end groups in the same generation, and type 2 HBPs have the end groups distributed over all generations. Both types make their own demands to the method of synthesis.

A mean-field theory for dendrimers, developed by Boris and Rubinstein[2] and refined by Evers et al.,[3] can be used to predict the size of HBPs. The free energy expression Evers et al.[3] used to predict the size of an uncharged dendrimer as a function of its number of generations is also adequate to relate the size of type 1 HBPs to their number of generations, despite some topological variety among HBPs of the same generation. It has been shown that in contrast to the situation for dendrimers the gyration radius R_g of type 1 HBPs of a fixed number of generations g with charged end groups varies between a lower limit and an upper limit, both of which can be calculated. This variety in R_g among charged type 1 HBPs is caused by topological variety that includes a variety in the number of (charged) end groups.

Type 2 HBPs are characterized by their degree of branching *DB*. The distribution of the end groups of these HBPs over the generations can be approximated by a normal distribution. The mean value $\langle g \rangle$ of this distribution is used in the mean-field calculations to obtain the gyration radius. To calculate the gyration radii of type 2 HBPs with charged free B groups, a new Coulombic term in the Helmholtz free energy has been derived.

The values of the gyration radii of simulated type 1 HBPs with only excluded-volume interactions are in agreement with the predictions of the mean-field theory. Small deviations, found for higher-generation HBPs, may be caused by an overestimation in the mean-field theory of the attractive interaction between the monomers. For these type 1 HBPs an increase in the number of generations (while keeping the number of monomers N constant) immediately results in an increase of the gyration radius. For charged type 1 HBPs agreement is found between gyration radii following from respectively the simulations and the mean-field theory. Small deviations may be attributed to the Helmholtz free energy term, which overestimates the stretching of the branches of the HBP. The size of charged type 1 HBPs of which both the number of monomers and the number of generations are known remains quite unpredictable because of topological variation that includes variation in the number of (charged) end groups. For both uncharged and charged type 2 HBPs the values of the gyration radii calculated in the simulations are similar to the values calculated in the mean-field theory. The radius of gyration of uncharged type 2 HBPs is hardly sensitive to variation of *DB*, whereas R_g of charged type 2 HBPs is a decreasing function of *DB*.

For HBPs with only excluded-volume interactions it is found that the relation between size and architecture of hyperbranched polymers is not given by a simple scaling law between R_g^2 and W, as proposed in the literature.[17] The scaling exponent reported by Sheridan, which is based on a huge amount of data (that covers a large part of the phase space), is probably some average of the scaling exponents that are found for the different regions in phase space.

From the radial mass distributions it can be concluded that type 1 HBPs with charged end groups exhibit an internal ordering. This ordering is most pronounced for dendrimers. As the number of generations increases, the ordering becomes weaker and finally vanishes (for $N = 94$ this is at $g_{max} = 10$). As the valence of the end groups is increased, the ordering becomes stronger. The radial mass distributions of type 2 HBPs of different degrees of branching are quite similar. The degree of branching has only a small influence on the width of the distributions. As a result, the number of monomers N becomes the only relevant topological parameter for these structures. The internal ordering observed in the mass distributions of HBPs with charged end groups manifests itself via oscillations in the static structure factor.

Acknowledgment. Grateful acknowledgment is made to A. A. Darinskii (Institute of Macromolecular Compounds, St. Petersburg), R. A. T. M. van Benthem (DSM Research and TU Eindhoven), and P. E. Fröling (DSM Research) for useful discussions. This work was carried out with the financial support of the NWO Grant 047.009.017.

Appendix A. $R_{g0}(g)$ for HBPs of Type 1

For ideal type 1 HBPs with a fixed number of beads N there is no one-to-one relation between the gyration

Figure 11. Type 1 HBPs with the same number of monomers N and the same number of generations g can still have a quite different connectivity. Here two extreme structures are given that belong to the collection of HBPs with $N = 94$ and $g = 10$: For the left structure $W = 46\,790$ and $R_{g0} = 2.30l$; for the right structure $W = 54\,240$ and $R_{g0} = 2.48l$.

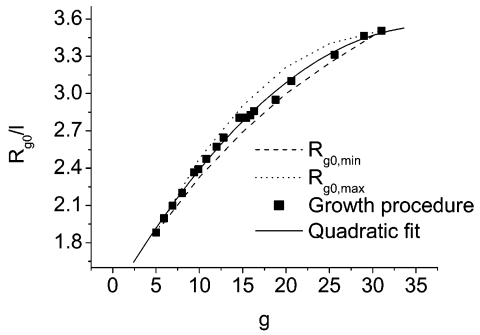

Figure 12. Minimal radius of gyration $R_{g0,\min}$ (dashed) and the maximal radius of gyration $R_{g0,\max}$ (dotted) as a function of the number of generations g for type 1 HBPs with 94 monomers. The data points (squares) concern type 1 HBPs that were built according to the generation growth procedure described in section 2. The solid curve represents a quadratic fit through these data points.

radius R_{g0} and the number of generations g. Fixing N and g still leaves some room for variation in the connectivity. This variation in the connectivity corresponds to a variation in the Wiener index W and therefore to a variation in R_{g0} (see eq 9). In Figure 11 the two extreme cases of the connectivity trees are displayed for type 1 HBPs with $N = 94$ and $g = 10$. For both structures the Wiener indices and the resulting values of R_{g0} are calculated. Despite the extreme difference in the connectivity of both structures, the difference in the gyration radius is only 7%. This is exactly the reason why it is still possible to give a good approximation of R_{g0} if the number of generations is known.

For a HBP of N monomers the minimum as well as the maximum value of R_{g0} (respectively indicated by $R_{g0,\min}$ and $R_{g0,\max}$) can be calculated as a function of the number of generations. This procedure is illustrated for a HBP of $N = 94$ monomers:

1. For the collections of HBPs with respectively $g =$ 5, 10, 15, 20, 25, and 31 generations both the structure with the smallest Wiener index $W_{\min}$ and the structure with the largest Wiener index $W_{\max}$ are created. (For the HBPs with $g = 10$ generations these structures are shown in Figure 11.) Subsequently, $W_{\min}$ and $W_{\max}$ are calculated using eq 2. Finally $R_{g0,\min}$ and $R_{g0,\max}$ are calculated from eq 9.

2. Via linear interpolation the values of $R_{g0,\min}(g)$ and $R_{g0,\max}(g)$ are found; both are plotted in Figure 12. The difference between both gyration radii is about 10% at most. The data points in Figure 12 concern type 1 HBPs that were built according to the generation-growth procedure described in section 2. For these structures g as well as N and W are known (and therefore, using eq 9, the value of R_{g0} is known). A quadratic fit (the solid curve in Figure 12) through these data points is used as relation $R_{g0}(g)$ for type 1 HBPs of $N = 94$. In the same way the relations $R_{g0}(g)$ for type 1 HBPs with $N = 10$, 22, 46, 190, and 382 are found.

Appendix B. Electrostatic Energy for Type 2 HBPs

The charge density inside a type 2 HBP with charged free B groups can be approximated by

$$\rho(r) = \frac{zN_{\mathrm{T}}}{\sigma_{\mathrm{c}}\sqrt{2\pi}} \frac{\exp\left(-\frac{1}{2}\left(\frac{r-\mu_{\mathrm{c}}}{\sigma_{\mathrm{c}}}\right)^2\right)}{4\pi r^2} \tag{27}$$

in which z is the effective charge of the free B groups, N_{T} the number of end groups, μ_{c} the mean the bead-to-core distance, and σ_{c} the standard deviation. The electrostatic energy of one free B group at position $\vec{r}'$ with respect to the core monomer is then given by

$$\frac{\Delta F_{Q/2}(r', \mu_{\mathrm{c}}, \sigma_{\mathrm{c}})}{k_{\mathrm{B}}T} = \lambda_{\mathrm{B}} \frac{z^2 N_{\mathrm{T}}}{\sigma_{\mathrm{c}}\sqrt{2\pi}} \int_V \frac{\exp\left(-\frac{1}{2}\left(\frac{r-\mu_{\mathrm{c}}}{\sigma_{\mathrm{c}}}\right)^2\right)}{4\pi|\vec{r} - \vec{r}'|} \exp(-\kappa|\vec{r} - \vec{r}'|)\, \mathrm{d}\vec{r} \tag{28}$$

where V is the smallest volume enclosing the whole HBP and κ is the inverse Debye screening length.

The factor $\exp(-\kappa|\vec{r} - \vec{r}'|)$ is negligible on the condition that the outer radius R of the HBP is much smaller than the Debye screening length ($R \ll \kappa^{-1}$), corresponding to solvents with (very) low ion concentrations. This condition is satisfied in this study ($\kappa^{-1} = 100l$). The other exponential factor can be simplified:

$$\exp\left(-\frac{1}{2}\left(\frac{r-\mu_{\mathrm{c}}}{\sigma_{\mathrm{c}}}\right)^2\right) = \begin{cases} 1 - \frac{1}{4}\left(\frac{r-\mu_{\mathrm{c}}}{\sigma_{\mathrm{c}}}\right)^2 & \mu_{\mathrm{c}} - 2\sigma_{\mathrm{c}} < r < \mu_{\mathrm{c}} + 2\sigma_{\mathrm{c}} \\ 0 & r < \mu_{\mathrm{c}} - 2\sigma_{\mathrm{c}} \text{ or } r > \mu_{\mathrm{c}} + 2\sigma_{\mathrm{c}} \end{cases} \tag{29}$$

After these simplifications the following expression is found for the electrostatic energy:

$$\frac{\Delta F_{Q/2}}{k_B T} = \lambda_b \frac{z^2 N_T}{\sigma_c \sqrt{2\pi}} \begin{cases} \ln\left(\frac{\mu_c + 2\sigma_c}{\mu_c - 2\sigma_c}\right) + 2\frac{\mu_c}{\sigma_c} - \frac{\mu_c^2}{2\sigma_c^2} \ln\left(\frac{\mu_c + 2\sigma_c}{\mu_c - 2\sigma_c}\right) & r' < \mu_c - 2\sigma_c \\ p(r', \mu_c, \sigma_c) & \mu_c - 2\sigma_c < r' < \mu_c + 2\sigma_c \\ \frac{16}{3}\frac{\sigma_c}{r'} & r' > \mu_c + 2\sigma_c \end{cases} \quad (30)$$

with

$$p(r',\mu_c,\sigma_c) = 2 - 2\left(\frac{\mu_c - 2\sigma_c}{r'}\right) + 2\ln\left(\frac{\mu_c + 2\sigma_c}{r'}\right) + \frac{1}{12r'\sigma_c^2}\left(r'^3 - 6r'^2\mu_c + 3r'\mu_c^2 + 2\mu_c^3 + 12r'\mu_c\sigma_c - 12r'\sigma_c^2 - 16\sigma_c^3 - 6r'\mu_c^2 \ln\left(\frac{\mu_c + 2\sigma_c}{r'}\right)\right)$$

The inner region ($r' < \mu_c - 2\sigma_c$) concerns a (charged) free B group that is enclosed by the spherically symmetric charge distribution; the Coulomb energy of such a group is independent of r' and will therefore not contribute to the expansion of the corresponding path of monomers. The intermediate region ($\mu_c - 2\sigma_c < r' < \mu_c + 2\sigma_c$) concerns a free B group within the charge distribution, while the outer region ($r' > \mu_c + 2\sigma_c$) concerns a free B group outside the charge distribution.

The total electrostatic energy of all charged B groups on a path of monomers is given by

$$\frac{\Delta F_{Q/2}(r'_1, ..., r'_n, \mu_c, \sigma_c)}{k_B T} = \frac{\Delta F_{Q/2}(r'_1, \mu_c, \sigma_c)}{k_B T} + ... + \frac{\Delta F_{Q/2}(r'_{n-1}, \mu_c, \sigma_c)}{k_B T} + 2\frac{\Delta F_{Q/2}(r'_n, \mu_c, \sigma_c)}{k_B T} \quad (31)$$

$r'_1 ... r'_n$ are the positions of the charged free B groups in the path that is considered. Note that the end monomer (at position r'_n) has two charged B groups. The exact positions of the charges along the contour length of the path are not important; the positions only have a weak influence on the prefactor of the electrostatic term in the free energy. In the mean-field calculations of this paper, the charges are assumed to be equally spaced.

References and Notes

(1) De Gennes, P. G.; Hervet, H. *J. Phys., Lett.* **1983**, *44*, 1351.
(2) Boris, D.; Rubinstein, M. *Macromolecules* **1996**, *29*, 7251.
(3) Lyulin, S. V.; Evers, L. J.; Van der Schoot, P.; Darinskii, A. A.; Lyulin, A. V.; Michels, M. A. J. *Macromolecules* **2004**, *37*, 3049.
(4) Lescanec, R. L.; Muthukumar, M. *Macromolecules* **1990**, *23*, 2280.
(5) Murat, M.; Grest, G. S. *Macromolecules* **1996**, *29*, 1278.
(6) Timoshenko, E. G.; Kuznetsov, Y. A.; Connolly, R. *J. Chem. Phys.* **2002**, *117*, 9050.
(7) Bosman, A. W.; Janssen, H. M.; Meijer, E. W. *Chem. Rev.* **1999**, *99*, 1665.
(8) Welch, P.; Muthukumar, M. *Macromolecules* **2000**, *33*, 6159.
(9) Rosenfeldt, S.; Dingenouts, N.; Ballauff, M.; Werner, N.; Vögtle, F.; Lindner, P. *Macromolecules* **2002**, *35*, 8098.
(10) Lyulin, A. V.; Davies, G. R.; Adolf, D. B. *Macromolecules* **2000**, *33*, 6899.
(11) Welch, P.; Muthukumar, M. *Macromolecules* **1998**, *31*, 5892.
(12) Widmann, A. H.; Davies, G. R. *Comput. Theor. Polym. Sci.* **1998**, *8*, 191.
(13) La Ferla, R. *J. Chem. Phys.* **1997**, *106*, 688.
(14) Nitta, K. *J. Chem. Phys.* **1994**, *101*, 4222.
(15) Wiener, H. *J. Am. Chem. Soc.* **1947**, *69*, 17.
(16) Lyulin, A. V.; Davies, G. R.; Adolf, D. B. *Macromolecules* **2001**, *34*, 3783.
(17) Sheridan, P. F.; Adolf, D. B.; Lyulin, A. V.; Neelov, I.; Davies, G. R. *J. Chem. Phys.* **2002**, *117*, 7802.
(18) Geladé, E. T. F.; Goderis, B.; De Koster, C. G.; Meijerink, N.; Van Benthem, R. A. T. M.; Fokkens, R.; Nibbering, N. M. M.; Mortensen, K. *Macromolecules* **2001**, *34*, 3552.
(19) Mendoza, C. I.; Marques, C. M. *Phys. Rev. E* **2002**, *66*, 051805.
(20) Aerts, J. *Comput. Theor. Polym. Sci.* **1998**, *10*, 73.
(21) Lee, A. T.; McHugh, A. J. *Macromolecules* **2001**, *34*, 7127.
(22) Allen, M. P.; Tildesley, D. J. *Computer Simulations of Liquids*; Clarendon Press: Oxford, 1987.
(23) Ermak, D. L.; McCammon, J. A. *J. Chem. Phys.* **1978**, *69*, 1352.
(24) De la Torre, J. G.; Rey, A.; Freire, J. J. *Macromolecules* **1987**, *20*, 342.
(25) Hölter, D.; Frey, H. *Acta Polym.* **1997**, *48*, 298.

MA049612K